The role of wave-induced Coriolis-Stokes forcing on the wind-driven mixed layer

JEFF A. POLTON, DAVID M. LEWIS*, AND STEPHEN E. BELCHER

Department of Meteorology, University of Reading, Berkshire, United Kingdom

(submitted 10 July 2003)

*Current affiliation: Department of Mathematics, University of Liverpool, Liverpool, United Kingdom.

Corresponding author address: S. E. Belcher. Department of Meteorology, University of Reading, PO Box 243, Reading, Berkshire RG6 6BB, United Kingdom. E-mail: s.e.belcher@reading.ac.uk

ABSTRACT

The interaction between the Coriolis force and the Stokes drift associated with ocean surface waves leads to a vertical transport of momentum, which can be expressed as a force on the mean momentum equation in the direction along wave crests. We investigate how this *Coriolis–Stokes forcing* affects the mean current profile in a wind-driven mixed layer, using simple models, results from large eddy simulations and observational data.

The effects of the Coriolis–Stokes forcing on the mean current profile is examined by re-appraising analytical solutions to the Ekman model that include the Coriolis–Stokes forcing. Turbulent momentum transfer is modelled using an eddy viscosity model, first with a constant viscosity, and second with a linearly varying eddy viscosity. Although the Coriolis–Stokes forcing penetrates only a small fraction of the depth of the wind-driven layer for parameter values typical of the ocean, the analytical solutions show how the current profile is substantially changed through the whole depth of the wind-driven layer. We show how, for this oceanic regime, the Coriolis–Stokes forcing supports a fraction of the applied wind stress, changing the boundary condition on the wind-driven component of the flow, and hence changing the current profile through all depths.

The analytical solution with the linearly varying eddy viscosity is shown to reproduce reasonably well the effects of the Coriolis–Stokes forcing on the current profile computed from large eddy simulations, which resolve the three-dimensional overturning motions associated with the turbulent Langmuir circulations in the wind-driven layer. Finally, the analytical solution with the Coriolis–Stokes forcing is shown to agree reasonably well with current profiles from historical observational data and certainly agrees much better than the

standard Ekman model. This finding provides compelling evidence that the Coriolis–Stokes forcing is an important mechanism in controlling the dynamics of the upper ocean.

1. Introduction

The fully-developed wind-driven current in the upper ocean is usually assumed to be a formed from a balance between Coriolis force and the divergence of vertical momentum transfer by turbulence stresses, as originally analysed by Ekman (see e.g. Mellor 1996). Wunsch (1996) has noted however, that at least in 1996 when he was writing, there was no observational evidence to support directly the Ekman model.

The oceanic wind-driven current profile is difficult to observe because the velocities are small and of similar magnitude to the velocities associated with inertial oscillations and surface wave motions. Nevertheless, observations suggest three features of the wind-driven current profile that need to be addressed. Firstly, the surface current lies at an angle of between 10^o and 45^o to the surface wind stress (Huang 1979). Secondly, at a depth between 5m and 20m the current is deflected by approximately 75^o to the wind stress (Price and Sundermeyer 1999). Thirdly, the current speed is rapidly attenuated with depth. The Ekman model cannot explain all these observed features (Lewis and Belcher 2003).

The difficulties in observation due to similarity in magnitude between the current speed and the speeds associated with other physical processes also suggests that other processes may be dynamically important. Surface waves are a ubiquitous feature of the ocean surface. The leading order water motions associated with the surface waves are periodic and do not affect the time-averaged, mean, current profile. Surface waves also produce, however, a mean Lagrangian transport in their direction of propagation, the Stokes drift (Phillips 1977), whose vertical variation is

$$u_s = U_s e^{2kz}, \qquad U_s = (ak)^2 c, \tag{1}$$

for wave amplitude a, wavenumber k, wave phase speed c and depth z that is zero at the mean sea level and decreasing downwards. The significance is that, in an inviscid fluid, lines of vorticity move with fluid parcels, and so the Stokes drift tilts and stretches initially vertical vorticity into the horizontal plane. In the ocean mixed layer there are two sources of vertical vorticity: vorticity from three-dimensional turbulent motions within the mixed layer, and planetary vorticity. Distortion of turbulent vorticity by Stokes drift is at the heart of models for Langmuir circulations (Leibovich 1983; Teixeira & Belcher 2002). The interaction of the Stokes drift with planetary vorticity is the subject of this paper.

The effects of Stokes drift in a rotating frame was first considered by Ursell (1950), Pollard (1970) and Hasselmann (1970) who showed that, for an inviscid ocean, there can be no net mass transport associated with the Stokes drift. Subsequently, also using a Lagrangian description, Weber (1983a,b) showed how including viscosity, no matter how small, actually yields a non-zero net mass transport. However, Hasselmann (1970) did show that the interaction between the planetary vorticity and the Stokes drift yields a force on the Eulerian momentum balance, namely $\boldsymbol{f} \times \boldsymbol{u_s}$. We refer to this forcing as the *Coriolis–Stokes forcing*. Madsen (1978) and Huang (1979) showed that this Coriolis–Stokes forcing acts in combination with the Coriolis force and the divergence of vertical momentum transfer by turbulent stresses, thereby changing the usual Ekman balance in the wind-driven mixed layer and the current profiles. Later studies have developed the theory for more sophisticated representations of the turbulent stress (Jenkins 1986, 1987), for finite depths (Xu and Bowen 1994), and for the role of Langmuir circulations (Gnanadesikan and Weller 1995). More recently McWilliams and Restrepo (1999) have shown that the depth integrated transport associated with the Coriolis–Stokes forcing can be comparable with the transport associated with the wind-forced Ekman transport, which suggests that the Coriolis–Stokes forcing is a signficant force in the upper ocean. Further evidence will be given here. A number of questions remain however.

Firstly, can the Coriolis–Stokes forcing, which penetrates only into shallow depths, affect the current profiles through its whole depth? If so then by what physical mechanism? Here we address these questions in section 3 by re-appraising the analytical solution for the current profile when the turbulent stress is parameterised simply. This analysis also then shows the parameters that control the magnitude of the changes to the current profile by the Coriolis–Stokes forcing.

Secondly, what evidence is there that the role of the Coriolis–Stokes forcing is real and measurable? This question is addressed here in two ways. Firstly, in section 4 the results of the simple models are compared with current profiles computed from large eddy simulations of the wind-driven ocean mixed layer that account for the effects of the Stokes drift. And secondly, in section 5 the results of the simple model are compared with recent observations of the wind-driven ocean mixed layer. We begin in section 2 with an interpretation of the Coriolis–Stokes forcing.

2. Stokes drift in a rotating frame

The Coriolis–Stokes forcing, $\boldsymbol{f} \times \boldsymbol{u_s}$, is a forcing by the surface waves on the mean flow. This term can be understood in two ways. First an intuitive interpretation. Vortex tubes are carried in the flow with fluid elements, and hence are transported by the Stokes drift. Since the Stokes drift varies with depth, vorticity that is initially vertical is tilted and stretched into the horizontal. There are several sources of this initially vertical vorticity. For example, random vorticity fluctuations associated with turbulence in the mixed layer have vertical components and when tilted and stretched these lead to elongated vortices in the streamwise direction, namely Langmuir circulations (Teixeira and Belcher 2002). Additionally, the planetary vorticity has a vertical component and hence can also interact with the Stokes drift, leading to the Coriolis–Stokes forcing, $\boldsymbol{f} \times \boldsymbol{u_s}$.

Alternatively, the $\boldsymbol{f} \times \boldsymbol{u_s}$ forcing can be interpreted as the divergence of a wave-induced stress that arises through modification by Coriolis acceleration of the orbital motions associated with the surface wave. The Eulerian velocity is decomposed into a rapidly-varying wave component, $\widetilde{\boldsymbol{u}}$, and a mean component, $\bar{\boldsymbol{u}}$. In a rotating ocean, the plane of the orbital motions associated with the surface wave is tilted in the along wave crest direction by the Coriolis acceleration, as shown schematically in Fig. 1.

[Figure 1 about here.]

This tilting introduces an along wave crest component into the Eulerian velocity field associated with the wave, namely $\widetilde{v}$. This component is correlated with the vertical component, $\widetilde{w}$, and hence yields a non-zero wave-induced stress, $\rho\overline{\widetilde{v}\widetilde{w}}$, when averaged over many wave cycles. As shown by Hasselmann (1970), the force associated with the divergence of this wave-induced stress can be expressed as

$$-\rho\frac{\partial}{\partial z}\overline{\widetilde{v}\widetilde{w}} = -\rho|\boldsymbol{f} \times \boldsymbol{u_s}|, \tag{2}$$

acting in the direction along wave crests. Hence the Eulerian motions in the upper part of the wind-forced mixed layer are subject to a $\boldsymbol{f} \times \boldsymbol{u_s}$ forcing arising from the interaction of the Coriolis acceleration with the Stokes drift associated with the surface waves. It is the effect of this Coriolis–Stokes forcing on mean current vertical profiles that is the focus of this paper.

3. Structure of the mean current profile in the Ekman–Stokes layer

When the Coriolis–Stokes forcing is introduced into the dynamics of the wind-driven mixed layer the structure of the mean current profile changes resulting in the *Ekman-Stokes layer*. Simple models are used to show how this forcing, which for parameters typical of the ocean acts only in a small upper fraction of the mixed layer, changes the currents over the whole depth of the layer.

The equations governing the mean, steady-state, ageostrophic current are given by

$$\rho f \hat{\mathbf{z}} \times (\boldsymbol{u} + \boldsymbol{u_s}) = \frac{\partial \boldsymbol{\tau}}{\partial z}, \tag{3}$$

where ρ is the density and $\boldsymbol{\tau}$ is the turbulent stress. This flow satisfies the following boundary conditions. Firstly, at the sea surface $z = 0$, a constant wind stress, $\boldsymbol{\tau_0}$, is applied in the x-direction:

$$\boldsymbol{\tau_0} = \rho u_*^2 \hat{\mathbf{x}}, \tag{4}$$

where u_* is the friction velocity. Secondly, at large depths, the turbulent stress and ageostrophic velocity tend to zero:

$$\boldsymbol{u} \to 0; \qquad \boldsymbol{\tau} \to 0 \qquad \text{as} \qquad z \to -\infty. \tag{5}$$

In this section the stress, $\boldsymbol{\tau}$, is parameterised with a simple gradient transfer eddy-viscosity model, namely

$$\boldsymbol{\tau} = \rho \kappa_m \frac{\partial \boldsymbol{u}}{\partial z}, \tag{6}$$

where κ_m is the eddy-viscosity.

There are two important depth scales in this problem. Firstly, there is the Stokes depth scale, δ_s, which scales as the depth of penetration of the Stokes drift, $\boldsymbol{u_s}$, and the $\boldsymbol{f} \times \boldsymbol{u_s}$ forcing. Secondly, there is the Ekman depth scale, δ_e, over which motion is influenced by the Earth's rotation. These are given by

$$\delta_s = \frac{1}{2k}; \qquad \delta_e = \sqrt{\frac{2\kappa_m}{f}}. \tag{7}$$

In the real ocean mixed layer δ_e (approximately $50\,\mathrm{m}$) is much greater than δ_s (approximately $5\,\mathrm{m}$). In this section we investigate solutions to (3) by (a) considering the depth integrated transport, then by considering solutions for (b) a constant eddy-viscosity κ_m and (c) a linearly varying eddy-viscosity κ_m.

a. Transport in the Ekman–Stokes layer

The depth-integrated transport gives a first indication of the relative magnitude of the wave forcing compared to the wind forcing. The transport is defined by

$$\boldsymbol{T} = \int_{-\infty}^{0} \boldsymbol{u}\, dz, \quad \boldsymbol{T_s} = \int_{-\infty}^{0} \boldsymbol{u_s}\, dz = \boldsymbol{U_s}\delta_s. \tag{8}$$

Integration of (3) and rearranging gives

$$\boldsymbol{T} + \boldsymbol{T_s} = -\frac{\hat{\mathbf{z}} \times \boldsymbol{\tau_0}}{f\rho}. \tag{9}$$

We define the Ekman-Stokes number, E_s (c.f. McWilliams and Restrepo 1999), to be a measure of the wave-forced transport compared to the wind-forced transport, namely

$$E_s = \frac{\text{wave-induced transport}}{\text{wind-induced transport}} = \frac{|\boldsymbol{T_s}|}{|\hat{\mathbf{z}} \times \boldsymbol{\tau_0}\rho f|} = \frac{U_s\delta_s}{U_e\delta_e}, \tag{10}$$

where U_e is the velocity scaling for the pure Ekman current, which is defined by the transport relation (8) and gives $U_e\delta_e = u_*^2/f$.

As a guide, we can express E_s in terms of the $10\,\mathrm{m}$ wind speed U_{10} (McWilliams and Restrepo 1999; Kenyon 1969). Kenyon (1969) fitted wave spectra data to deduce coefficients for an empirical formula of u_s, based on the Pierson and Moskowitz (1964) fully developed sea model, as a function of wind speed at $19.5\,\mathrm{m}$. McWilliams and Restrepo (1999) used this to calculate E_s (implicitly approximating the $19.5\,\mathrm{m}$ wind speed to be U_{10}). Here, assuming a log profile for the wind speed, we present a corrected expression for E_s as a function of U_{10} that is given by

$$E_s = 0.39 \frac{f U_{10}}{c_D} \left(1 + \frac{c_D^{1/2} \ln 1.95}{\kappa} \right)^3, \tag{11}$$

where c_D is the atmospheric drag coefficient defined by $\tau_0 = \rho_a c_D U_{10}^2$, with air density $\rho_a = 1.2\,\mathrm{kg\,m^{-3}}$. The expression for c_D is taken from Garratt (1992, equation 4.24),

$$c_D = (0.75 + 0.067 U_{10}) \times 10^{-3}. \tag{12}$$

Fig. 2 shows how E_s increases with wind speed for 4 different latitudes. For example, at a latitude of $50°$N, $E_s(U_{10} = 12\,\mathrm{m\,s^{-1}}) = 0.4$ suggesting that the wave-induced transport can be a significant fraction of the wind-induced transport. This finding motivates analysis of the effects of the Coriolis–Stokes forcing on the current profile in the Ekman–Stokes layer, which is considered next.

[Figure 2 about here.]

b. Current profile with a constant eddy-viscosity

Just as for the classical Ekman layer, many of the characteristics of the current in the Ekman–Stokes layer are shown in the solution to the dynamical equations with a constant eddy viscosity κ_m. This problem was first considered by Madsen (1978) and Huang (1979). Here we re-appraise the solution by writing it in a form that highlights how the shallow wave process can change the current profile over the whole depth of the Ekman–Stokes layer.

The solution in this case is obtained by recasting the momentum equation (3) into complex notation, where $\boldsymbol{u} = u\mathbf{i} + v\mathbf{j}$ is re-expressed as $\mathcal{U} = u + iv$. The solution to (3) can be written as

$$\mathcal{U} = \mathcal{U}_e + \mathcal{U}_{es} + \mathcal{U}_s, \tag{13}$$

where

$$\begin{aligned}
\mathcal{U}_e &= (1-i)U_e \mathit{exp}\left\{(1+i)\frac{z}{\delta_e}\right\}, & (14)\\
\mathcal{U}_{es} &= (1-i)U_e \mathit{exp}\left\{(1+i)\frac{z}{\delta_e}\right\}\left(\frac{1}{2}\frac{U_s/\delta_s}{U_e/\delta_e}\frac{1}{(1+i\frac{1}{2}\frac{\delta_e^2}{\delta_s^2})}\right), & (15)\\
\mathcal{U}_s &= -\frac{U_s}{(1+i\frac{1}{2}\frac{\delta_e^2}{\delta_s^2})}\mathit{exp}\left\{\frac{z}{\delta_s}\right\}. & (16)
\end{aligned}$$

Here $\mathcal{U}_e$ is the pure Ekman solution and would be the only solution if the wave-induced affects were not included. However, the Stokes-Coriolis forcing introduces two new terms into the solution. Firstly, there is a Stokes component of the current, $\mathcal{U}_s$. This part of the solution is forced directly by the Coriolis–Stokes force; mathematically it arises as a particular integral solution to the Coriolis–Stokes forcing. The Stokes component of the current decays over the Stokes depth scale, δ_s. (The Stokes component of the current $\mathcal{U}_s$ is the dynamical response to the Coriolis–Stokes forcing and should not be confused with the Stokes drift, u_s). Secondly, there is an Ekman-Stokes component of the current, $\mathcal{U}_{es}$. Importantly, this term decays over the Ekman depth scale, δ_e, and so changes the current profile through the whole depth of the layer. This part of the solution arises to ensure that the solution satisfies the wind-stress boundary condition imposed at the sea surface. That is, the Stokes component of the solution carries some of the wind stress supplied at the surface, hence the stress carried by the Ekman-type components of the solution changes to satisfy the boundary condition. In this sense the effect of the waves is to change the boundary condition on the Ekman current.

The decomposition of the solution (14)-(16) is shown in a hodograph and as depth profiles in Fig. 3. The thick lines represent the full solution, the thin solid lines represent the Ekman component, the dashed lines denote the Ekman-Stokes component and the dotted-dashed lines denote the Stokes current component. Notice how the Ekman-Stokes component of the solution penetrates through the whole depth of the wind-driven layer, whereas the Stokes component of the solution penetrates only the upper fraction of the layer. The wave-induced effect is to further rotate the current vectors, as compared with the pure Ekman solution.

[Figure 3 about here.]

Here we are particularly interested in the Ekman-Stokes term, as this has the same depth structure as the pure Ekman term and so penetrates the whole depth of the layer. So consider the ratio, R, of the Ekman-Stokes current to the pure Ekman current, which is given by

$$R = \frac{|\mathcal{U}_{es}|}{|\mathcal{U}_e|} = \frac{1}{2}\frac{U_s/\delta_s}{U_e/\delta_e}\left|\frac{1}{1+i\frac{1}{2}\frac{\delta_e^2}{\delta_s^2}}\right|. \tag{17}$$

There are two limiting cases.

Firstly, consider the case when $\delta_e \gg \delta_s$, so that the Stokes component of the current decays rapidly within the upper portion of the Ekman–Stokes layer. This is the limit that is typical of the real ocean mixed layer. In this case $|1 + i\frac{1}{2}\delta_e^2/\delta_s^2| \approx \frac{1}{2}\delta_e^2/\delta_s^2$, so that

$$R \approx \frac{U_s\delta_s}{U_e\delta_e} = E_s. \tag{18}$$

Hence, when $\delta_e \gg \delta_s$, the ratio of the Ekman-Stokes to Ekman component of the current is the ratio of the wave-induced transport to wind-induced transport, E_s. That is, in this case, the wave-driven transport is carried by the Ekman-Stokes part of the solution, and is carried over the Ekman depth.

Secondly, consider the case when $\delta_e \ll \delta_s$. This limit of a thin Ekman boundary layer with a deeper Stokes layer might be generated in a laminar Ekman–Stokes layer when the viscosity is small, such as might be produced in a laboratory experiment. In the ocean this regime might represent swell propagation over a shallow wind-driven layer. In this case $|1 + i\frac{1}{2}\delta_e^2/\delta_s^2| \approx 1$ so that

$$R = \frac{1}{2}\frac{U_s/\delta_s}{U_e/\delta_e}, \tag{19}$$

which is a scaling for a ratio of the gradients of the Stokes to the Ekman components. To understand the physics behind this balance, consider the surface stress boundary condition for the flow (4) and (6), which can be rewritten as

$$\frac{\partial \mathcal{U}}{\partial z} = \frac{u_*^2}{\kappa_m} = 2\frac{U_e}{\delta_e} \qquad \text{at} \qquad z = 0. \tag{20}$$

Equation (14) shows that the pure Ekman current shear satisfies this boundary condition. Hence the Ekman-Stokes component, $\mathcal{U}_{es}$, of the solution is required to give a surface shear that is equal and opposite to the shear in the Stokes component, $\mathcal{U}_s$, of the current. When $\delta_e \ll \delta_s$ the magnitude of the Stokes contribution in (16) is at its greatest. Hence, the gradient of the Stokes current shear is U_s/δ_s. Rewriting R as the ratio of the Ekman-Stokes component's gradient, U_s/δ_s, to the Ekman component's gradient (20) we recover (19).

Note, however, that in this regime small R does not necessarily imply that E_s must be small since $R = 0.5E_s(\delta_e/\delta_s)^2$. For example, taking $f = 1 \times 10^{-4}\,\mathrm{s}^{-1}$, a smaller eddy viscosity coefficient $\kappa_m = 1 \times 10^{-3}\,\mathrm{m}^2\,\mathrm{s}^{-1}$, $u_* = 6.1 \times 10^{-3}\,\mathrm{m\,s}^{-1}$ and $a = 1.3\,\mathrm{m}$ and $k = 0.042\,\mathrm{m}^{-1}$, such that $\delta_s = 11.9\,\mathrm{m} > \delta_e = 4.5\,\mathrm{m}$, then $R = 0.10$ and $E_s = 1.5$.

c. Linearly varying eddy-viscosity

A more quantitatively accurate model for the turbulent Ekman–Stokes layer can be constructed with an eddy-viscosity that varies linearly with depth, so that

$$\kappa_m(z) = -\kappa u_* z = \kappa u_* z_+, \tag{21}$$

when $z < 0$ and $\kappa = 0.4$ is the von Karman constant, and $z_+ = -z$.

The momentum equations then reduce to

$$\frac{\partial}{\partial \zeta}\left(\zeta \frac{\partial \mathcal{U}}{\partial \zeta}\right) - \zeta \mathcal{U} = \zeta u_s, \tag{22}$$

where $\zeta^2 = i\frac{4f}{\kappa u_*} z_+$. The particular solution is obtained by the method of variation of parameters, giving (following Madsen 1977; Lewis and Belcher 2003)

$$\mathcal{U} = \left\{ \frac{2u_*}{\kappa} + 4i \int_0^{\hat{z}_+} I_0(\sqrt{8it})\hat{u}_s(t)\,dt \right\} K_0(\zeta) + 4iI_0(\zeta) \int_{\hat{z}_+}^{\infty} K_0(\sqrt{8it})\hat{u}_s(t)\,dt, \tag{23}$$

where I_0 and K_0 are modified Bessel functions (Abramowitz and Stegun 1972),

$\hat{z}_+ = z_+/\delta_e, \quad \delta_e = 2\kappa u_*/f,$ and $\hat{u}_s(t) = U_s \exp(-t\delta_e/\delta_s)$.

In the limits that $\delta_e/\delta_s \gg 1$ and $|z| \gg \delta_s$, the solution simplifies to

$$\mathcal{U} \approx \frac{2u_*}{\kappa}\left\{1 - i\frac{U_s\delta_s}{U_e\delta_e}\right\} K_0(\zeta). \tag{24}$$

Hence the ratio R (17) of the Ekman-Stokes component to the wind-driven Ekman component is again given by E_s, the ratio of wave- to wind-induced transports. This is in agreement with the value found with the constant eddy-viscosity case. This agreement is no accident. In this limit of $\delta_e/\delta_s \gg 1$, the Stokes response (the last term in (23)) to the $\boldsymbol{f} \times \boldsymbol{u_s}$ forcing is negligible (as is the corresponding contribution to the net transport). Hence the wave-induced Eulerian transport, which has to equal $-\boldsymbol{T_s}$ by the integral constraint (9), must be carried by the Ekman-Stokes component of the solution. Hence $R = E_s$. The significance, is that in this limit of $\delta_e/\delta_s \gg 1$, which is the limit appropriate for much of the ocean mixed layer, the Eulerian transport associated with the $\boldsymbol{f} \times \boldsymbol{u_s}$ forcing is carried through the same depth as the wind-driven Ekman solution. And we have shown here that this result must follow through independently of the eddy-viscosity model used to compute the turbulent stress.

d. Effective boundary condition for a shallow wave forcing

Above it was shown how in the limit of $\delta_e/\delta_s \gg 1$, when the Ekman–Stokes layer is deep compared to the depth of the Coriolis-Stokes forcing, $\boldsymbol{f} \times \boldsymbol{u_s}$, the effect of the forcing on the current profile reduces to a canonical form. We now develop an argument to show how this can be understood as the Coriolis-Stokes forcing changing the boundary condition on the wind-driven layer.

Recall that the Coriolis-Stokes forcing arises from a stress caused by the motions associated with the surface wave, see (2). Hence the momentum equation governing the wind-driven layer can be written

$$\rho f \hat{\mathbf{z}} \times \boldsymbol{u} = \frac{\partial \boldsymbol{\tau_{tot}}}{\partial z}, \tag{25}$$

where the total stress, $\boldsymbol{\tau_{tot}}$ is the sum of the turbulent stress $\boldsymbol{\tau}$ and a wave-induced stress, associated with a wave train propagating in the direction of $\boldsymbol{u_s}$. In the limit of $\delta_e/\delta_s \gg 1$, the wave-induced stress tends to zero beneath the surface and hence the Ekman–Stokes layer can be modelled using standard Ekman theory (25) subject to the following boundary conditions

$$\boldsymbol{\tau_{tot}} = \rho u_*^2 \left(\hat{\boldsymbol{\tau}}_{\mathbf{0}} - \hat{\mathbf{z}} \times \hat{\boldsymbol{u}}_{\boldsymbol{s}} E_s\right) \quad \text{on } z = 0, \qquad \boldsymbol{u} \to 0 \quad \text{as } z \to -\infty, \tag{26}$$

for arbitrary wind and wave directions (with hats denoting unit vectors). This finding may have implications for representation of the Coriolis–Stokes term in ocean general circulation models. These models do not typically have sufficient vertical resolution to compute the flow within the upper part of the mixed layer where the Coriolis–Stokes force acts. The present analysis shows that the effect of this forcing on the mixed layer can be represented by changing the boundary condition on the standard Ekman equations.

4. Large eddy simulation of the Ekman–Stokes layer

We have developed simple models for the wind-driven mixed layer that show how the Coriolis–Stokes force changes the mean current profile through all depths. These models represented the turbulent stress associated with three-dimensional overturning turbulent motions through simple eddy-viscosity models. These turbulent motions are represented more faithfully through large eddy simulation (hereafter LES), where the fully nonlinear equations of motion are integrated forward in time with sufficient resolution to compute explicitly the large-scale turbulent motions. The small-scale turbulence is parameterised. In this section the mean current profiles are computed by an LES model of the turbulent Ekman–Stokes layer.

Following Skyllingstad and Denbo (1995) and McWilliams et al. (1997), we perform LES of the wave filtered Craik-Leibovich equations to account for wave-length averaged effects of surface waves. With this procedure the momentum equation becomes

$$\frac{D\boldsymbol{u}}{Dt} + \boldsymbol{f} \times (\boldsymbol{u} + \boldsymbol{u_s}) = -\nabla\pi + \boldsymbol{u_s} \times \boldsymbol{\omega} + SGS. \tag{27}$$

Here $\boldsymbol{u}$ is the wave-averaged Eulerian velocity, $\boldsymbol{f} = f\hat{\mathbf{z}}$ is the Coriolis parameter, $\hat{\mathbf{z}}$ is the upward unit vector, $\boldsymbol{\omega} = \nabla \times \boldsymbol{u}$ is the local vorticity vector and $D/Dt = \partial/\partial t + \boldsymbol{u} \cdot \nabla$ is the material derivative. The subgrid scale processes (denoted SGS) are parameterised using a standard Smagorinsky model. Finally, π is the generalised pressure given by

$$\pi = \frac{p}{\rho_0} + \frac{1}{2}(|\boldsymbol{u} + \boldsymbol{u_s}|^2 - |\boldsymbol{u}|^2). \tag{28}$$

We consider the simplest problem when the density is prescribed to be constant with depth.

The governing equations then contain the Coriolis–Stokes forcing, $\boldsymbol{f} \times \boldsymbol{u_s}$, and also the *vortex force*, $\boldsymbol{u_s} \times \boldsymbol{\omega}$, which represents the straining of the vorticity associated with resolved mean and turbulent motions by the Stokes drift. This latter term gives rise to Langmuir circulations (Leibovich 1983), which lead to enhanced vertical mixing. The LES with the vortex force yields a turbulent boundary layer with elongated Langmuir vortices on a range of scales, whose dynamics are described in Skyllingstad and Denbo (1995), McWilliams et al. (1997) and Teixeira and Belcher (2003). Here we focus on the mean current profiles produced by the LES.

The equations are integrated numerically using a code based on the atmospheric boundary layer code BLASIUS (Wood and Mason 1993), which has been adjusted to include the two wave forcing terms. The code is run in LES mode (Brown et al. 2001) using a Smagorinsky subgrid model. For further model details refer to Wood et al. (1998). The domain is periodic and isotropic in the horizontal directions spanning $120\,\mathrm{m}$ with a resolution of $3\,\mathrm{m}$. In the vertical direction 200 grid points span $90\,\mathrm{m}$ with a resolution of $0.46\,\mathrm{m}$. This is similar to the $3\,\mathrm{m} \times 3\,\mathrm{m} \times 0.6\,\mathrm{m}$ resolution used by McWilliams et al. (1997), which is vertically uniform. Our model also has a uniform vertical resolution except in the upper $1\,\mathrm{m}$ where we use a stretched grid over 4 levels. The most significant difference between our simulations are those of McWilliams et al. (1997) is in the stratification. In the McWilliams et al. (1997) study, the upper $33\,\mathrm{m}$ is neutrally buoyant and the rest is stably statified. We simplify the study by making the whole domain neutrally buoyant. At the surface a constant wind-stress is applied in the x-direction such that at $z = -z_0$,

$$\kappa_m \frac{\partial u}{\partial z} = u_*^2; \qquad \kappa_m \frac{\partial v}{\partial z} = 0 \tag{29}$$

where κ_m is the mixing-length eddy viscosity, which parameterises the stress very near the surface, u_* is the friction velocity, and z_0 is the roughness length. At the lower boundary a no-flow condition is imposed. The code was checked by performing a simulation with the parameters of McWilliams et al. (1997). Results for the mean flow and turbulence statistics from our simulation (not shown) are in good agreement with McWilliams et al. (1997).

A total of 16 simulations have been performed for a range of k and U_s wave parameters. Each of the simulations had $u_* = 6.1 \times 10^{-3}\,\mathrm{m\,s^{-1}}$ (corresponding to a $10\,\mathrm{m}$ atmospheric wind speed, $U_{10} \approx 5\,\mathrm{m\,s^{-1}}$), $f = 1 \times 10^{-4}\,\mathrm{s^{-1}}$ and $z_0 = 0.1\,\mathrm{m}$. The wave parameters are $k = 0.02625, 0.0525, 0.105, 0.210\mathrm{m^{-1}}$, which yields wavelength $\lambda = 240, 120, 60, 30\,\mathrm{m}$, and a surface Stokes drift of $U_s = 0, 0.017, 0.034, 0.068, 0.271\,\mathrm{m\,s^{-1}}$. Each run is integrated to $90\,000\,\mathrm{s}$ (including an inertial spin up time of $O(1/f) \sim 10^4\,\mathrm{s}$). Starting at $5000\,\mathrm{s}$, mean flow and turbulent statistics are computed from instantaneous horizontal averages that are taken approximately every $10\,\mathrm{s}$.

a. LES results and comparison with eddy-viscosity closure model

The mean current profiles obtained from the LES are now compared with the simple eddy-viscosity closure model discussed in section 3c. Fig. 4 shows solutions from four simulations, all with $k = 0.0525\,\mathrm{m^{-1}}$ ($\lambda = 120\,\mathrm{m}$) but with increasing wave amplitudes, and hence increasing U_s. (Since $E_s \propto U_s/2k$, increasing k has the same qualitative effect as decreasing U_s).

[Figure 4 about here.]

The upper panels show hodographs of the locus of the current vector as the depth increases. The middle panels show corresponding profiles of mean along-wind velocity, $\bar{u}$ against depth. The lower panels show the corresponding mean across-wind velocity, $\bar{v}$, against depth. In each panel the thicker solid line is the LES data, the thinner sold line is the solution from the model with linearly-varying eddy-viscosity closure and the dashed line is LES data from a run without wave forcing (that is the pure Ekman solution).

First consider the LES solutions. Even for moderate values of the Stokes drift, for example when $a = 0.95\,\mathrm{m}$ so that $ak = 0.05$ and $U_s = 0.034\,\mathrm{m\,s^{-1}}$, the LES with wave forcing is markedly different from the pure Ekman solution without wave forcing. The effect of the Coriolis–Stokes force is primarily to rotate the current profiles southwards, consistent with the effective boundary condition ideas in section 3d.

Comparing the LES solutions with the solution from the model with linearly-increasing eddy-viscosity we see that there is a reasonably good quantitative agreement, particularly within the bulk of the Ekman–Stokes layer. Very close to the surface, within the layer affected directly by the Coriolis–Stokes forcing, $|z| < \delta_s \approx 10m$, the LES shows less shear than the solution from the closure model. It seems likely that the enhanced mixing due to the Langmuir circulations, which are undoubtedly present in the LES, reduce the shear there. The eddy-viscosity model has a prescribed linearly varying eddy-viscosity, which makes no attempt to represent these Langmuir circulations. Nevertheless, these comparisons show that the Coriolis–Stokes forcing leads to significantly changed mean current profiles and that the closure model represents this effect throughout the bulk of the mixed layer.

5. Evidence for effects of Coriolis–Stokes forcing in observational data

In this section we compare the simple analytical model, used in the LES comparisons, with long-term observations of the upper ocean. We will find that the observational data is explained by the model much better when the Coriolis–Stokes forcing is included.

Extraction of the mean wind-driven current profile from the background of wave motions, inertial oscillations and geostrophic eddies requires sophisticated and sensitive instruments that can be deployed for long periods. Consequently it is only relatively recently that data sets have been collected that can be compared with models of the wind-driven current. Here we use data described in Price and Sundermeyer (1999).

The LOTUS3 data, ’Long Term Upper Ocean Study’, (Briscoe and Weller 1984; Price et al. 1987) was collected from a surface mooring in the Western Sargasso Sea ($34°$N, $70°$W) spanning 160 days during the summer months of 1982. Vector Measuring Current Meters and a buoy mounted meteorological mast were used to record ocean currents and wind velocity. The data is processed by first subtracting the geostrophic velocity (the velocity at some depth deeper than the wind penetration depth, which in this case is taken as $50\,\mathrm{m}$). Secondly, since the wind direction was not steady over the 160 day period, daily averages of wind and current were rotated such that the wind was aligned with an arbitrary north. This daily data was then averaged over the 160 days.

The EBC data - ’Eastern Boundary Current’, is reported in Chereskin (1995). This data set is taken from a mooring $400\,\mathrm{km}$ off the coast of North California ($37°$N, $128°$W) and was collected, over a 6 month period from April 8th to October 20th 1993, using ADCP and buoy wind observations. The data required no rotating prior to averaging as the wind was unidirectional over the 6-month collecting period.

Price and Sundermeyer (1999) also describe a third data set, the TPHS data, ’Transpacific Hydrographic Section’, that was originally reported in Wijffels et al. (1994). Again this data was processed using the same procedure as described for the LOTUS3 data (see Price and

Sundermeyer 1999, for details). However, since the Coriolis parameter is much smaller and the corresponding depth scales are larger (the wind penetration depth is $150\,\mathrm{m}$) the linearly varying eddy-viscosity and uniform density assumption break down (Lewis and Belcher 2003) and so we consider this data set no further.

Since no observations of surface waves were made with the current and wind measurements Lewis and Belcher (2003) use empirical formulae to deduce U_s and k from the observed wind stress as a function of fetch and for a fully developed sea (FDS). They also develop a coupled linear eddy-viscosity closure ocean-atmosphere model to deduce z_0 from the wind stress. Here we take a more pragmatic approach to deduce the values of unknown parameters. Firstly, the atmospheric component to the model is not used because the results are not particularly sensitive to z_0 provided it lies within the range $10^{-4}\,\mathrm{m}$ to $10^{-3}\,\mathrm{m}$. Secondly, all the observation sites are sufficiently far from land that the waves cannot be fetch limited and so we assume here for simplicity that the waves are fully developed and that the peak frequency ω and the significant wave height a are the appropriate terms in the expression for Stokes drift (c.f. equations 6.71a-b Komen et al. 1994):

$$\frac{g^2\rho^2a^2}{16\rho_a^2u_*^4} = 1.1\times10^3, \quad \frac{\sigma u_*}{2\pi g}\left(\frac{\rho}{\rho_a}\right)^{0.5} = 5.6\times10^{-3}. \tag{30}$$

Finally, we vary the key wave parameters, k and U_s, to examine the sensitivity of the results to the wave properties.

[Figure 5 about here.]

Fig. 5 shows hodographs of the current vector for the LOTUS3 and EBC data. The solutions from the analytical model with linearly-varying eddy viscosity and accounting for the Coriolis–Stokes force (the solid line) show strikingly good agreement with the measurements. The results of the model when the Coriolis–Stokes force is set to zero (the dashed line) does not agree well. Also shown is the range that the hodograph from the theory can take when the wave parameters are varied. The solid shading denotes the range of solutions from the model when the wavelength of the waves is changed by $\pm 100\%$. The hatched envelope arises from changing the square of the wave amplitude, and hence U_s, by $\pm 50\%$. The observational data all lie within these bounds, whereas the pure Ekman solution lies some distance outside.

We acknowledge the suggestion of Price and Sundermeyer (1999) that diurnal variation in the depth of the layer could explain the deviation from the pure Ekman solution. As pointed out by Lewis and Belcher (2003) this approach, however, yields a surface current whose angle to the surface wind is outside the range of observations.

Hence the comparisons provide compelling evidence that the Coriolis–Stokes force produces measurable changes to wind-driven current profiles.

6. Concluding Remarks

We have examined the role of the Coriolis–Stokes forcing, $\boldsymbol{f} \times \boldsymbol{u_s}$, in shaping the mean current profile in the wind-driven ocean mixed layer. At first sight this force might be thought to be small, since it involves the Stokes drift, which scales on the wave slope squared. Estimates show that in conditions of even modest sea state the depth-integrated transport associated with this forcing can be a considerable fraction of the depth-integrated wind-driven transport. This observation motivated the present more detailed examination of the role of this forcing.

Simple analytical solutions, based on parameterising the turbulence using simple eddy-viscosities, show how the Coriolis–Stokes forcing interacts with the Coriolis force and the turbulent stress divergence. The resulting wind-driven current profile is characterised by two length scales, namely the depth scale of the wind-driven layer, δ_e, and the depth of penetration of the Coriolis–Stokes forcing, δ_s. In typical ocean conditions $\delta_s \ll \delta_e$, and yet the current profile is completely changed through all depths, with the current vectors rotated further away from the direction of the wind stress. The reason is that the Coriolis–Stokes forcing absorbs a fraction of the applied wind stress, thus changing the effective boundary condition on the standard wind-driven Ekman solution. A corollary to this finding is that the effects of the Coriolis–Stokes forcing can be represented simply by changing the boundary condition on the standard equations of motion. Hence there is no need for numerical ocean models to resolve explicitly the region affected directly by the Coriolis–Stokes forcing.

We investigated the relevance of these findings to the real ocean by comparing the results of the simple models to large eddy simulations (LES) and observations. The LES resolve the large-scale turbulent motions, but represent the effects of the waves through their wavelength averaged effects only. Nevertheless, the wind and wave conditions are prescribed and remain constant, giving clean data to compare with the simple theory. The observational data, taken from the LOTUS3 and EBC campaigns, on the other hand, contain the complexity of the real world, including variable wind speed and direction. Wave properties were not measured during the observations and so were estimated here by assuming that the waves were fully developed with respect to the local wind speed. When compared to both the LES and the observations the simple models that account for the Coriolis–Stokes forcing have shown encouraging agreement. This provides perhaps the first evidence of the signature of the Coriolis–Stokes forcing in observations. These findings suggest that future observations of the wind-driven mixed layer also need to measure surface wave properties.

Ultimately it is the wind that provides the momentum flux to the surface wind-stress, with its wind-driven flow, and to the surface waves, with their associated the Coriolis–Stokes forcing. In the present paper the wind and waves have been specified separately. An important topic for future research will therefore be to examine the partition of the momentum flux between these two components.

Acknowledgments. The research presented in this paper was funded by the Leverhulme Trust under grant F/00239/A and the US Office of Naval Research under grant N-00014-01-1-0133.

References

Abramowitz, M., and I. A. Stegun, 1972: *Handbook of Mathematical Functions*, Dover Publications, Inc., New York. 1046pp.

Briscoe, M. G., and R. A. Weller, 1984: Preliminary results from the Long-Term Upper-Ocean Study (LOTUS). *Dyn. Atmos. Oceans*, **8**, 243–265.

Brown, A. R., J. M. Hobson, and N. Wood, 2001: Large-eddy simulation of neutral turbulent flow over rough sinusoidal ridges. *Boundary-Layer Meteorol.*, **98**, 411–441.

Chereskin, T. K., 1995: Direct evidence for an Ekman balance in the California Current. *J. Geophys. Res.*, **100**, 18261–18269.

Garratt, J. R., 1992: *The atmospheric boundary layer*. Cambridge University Press, 316pp.

Gnanadesikan, A., and R. A. Weller, 1995: Structure and instability of the Ekman spiral in the presence of surface gravity waves. *J. Phys. Oceanogr.*, **25**, 3148–3171.

Hasselmann, K., 1970: Wave-driven inertial oscillations. *Geophysical Fluid Dynamics*, **1**, 463–502.

Huang, N. E., 1979: On surface drift currents in the ocean. *J. Fluid Mech.*, **91**, 191–208.

Jenkins, A. D., 1986: A theory for steady and variable wind- and wave-induced currents. *J. Phys. Oceanogr.*, **16**, 1370–1377.

—, 1987: Wind and wave induced currents in a rotating sea with depth-varying eddy viscosity. *J. Phys. Oceanogr.*, **17**, 938–951.

Kenyon, K. E., 1969: Stokes drift for random gravity waves. *J. Geophys. Res.*, **74**, 6991–6994.

Komen, G. J., L. Cavaleri, M. Donelan, K. Hasselmann, S. Hasselmann, and P. A. E. M. Janssen, 1994: *Dynamics and Modelling of Ocean Waves*, Cambridge Univesity Press. 1st edition, 532pp.

Leibovich, S., 1983: The form and dynamics of Langmuir circulations. *Ann. Rev. Fluid Mech.*, **15**, 391–427.

Lewis, D. M., and S. E. Belcher, 2003: Time-dependent, coupled, Ekman boundary layer solutions incorporating Stokes drift. *Dyn. Atmos. Oceans*, submitted.

Madsen, O. S., 1977: A realistic model of the wind-induced Ekman boundary layer. *J. Phys. Oceanogr.*, **7**, 248–255.

—, 1978: Mass transport in deep-water waves. *J. Phys. Oceanogr.*, **8**, 1009–1015.

McWilliams, J. C., P. P. Sullivan, and C.-H. Moeng, 1997: Langmuir turbulence in the ocean. *J. Fluid Mech.*, **334**, 1–30.

—, and J. M. Restrepo, 1999: The wave-driven ocean circulation. *J. Phys. Oceanogr.*, **29**, 2523–2540.

Mellor, G. L., 1996: *Introduction to Physical Oceanography*. American Institute of Physics, Woodbury, NY., 260pp.

Phillips, O. M., 1977: *Dynamics of the Upper Ocean*. Cambridge University Press, 336 pp.

Pierson, W. J., and L. Moskowitz, 1964: A proposed spectral form for fully developed wind seas based on the similarity theory of S. A. Kitaigorodskii. *J. Geophys. Res.*, **69**, 5181–5203.

Pollard, R. T., 1970: Surface waves with rotation: An exact solution. *J. Geophys. Res.*, **75**, 5895–5898.

Price, J. F., R. A. Weller, and R. R. Schudlich, 1987: Wind-Driven Ocean Currents and Ekman Transport. *Science*, **238**, 1534–1538.

—, and M. A. Sundermeyer, 1999: Stratified Ekman layers. *J. Geophys. Res.*, **104**, 20467–20494.

Skyllingstad, E. D., and D. W. Denbo, 1995: An ocean large-eddy simulation of Langmuir circulations and convection in the surface mixed layer. *J. Geophys. Res.*, **100**, 8501–8522.

Teixeira, M. A. C., and S. E. Belcher, 2002: On the distortion of turbulence by a progressive surface wave. *J. Fluid Mech.*, **458**, 229–267.

—, and —, 2003: On the structure of Langmuir turbulence. *J. Fluid Mech.*, (submitted).

Ursell, F., 1950: On the theoretical form of ocean swell on a rotating earth. *Mon. Not. Roy. Astron. Soc. Geophy. Suppl.*, **6**, 1–8.

Weber, J. E., 1983a: Attenuated wave-induced drift in a viscous rotating ocean. *J. Fluid Mech.*, **137**, 115–129.

—, 1983b: Steady wind- and wave-induced currents in the open ocean. *J. Phys. Oceanogr.*, **13**, 524–530.

Wijffels, S., E. Firing, and H. Bryden, 1994: Direct Observations of the Ekman Balance at 10°N in the Pacific. *J. Phys. Oceanogr.*, **24**, 1666–1679.

Wood, N., and P. Mason, 1993: The pressure force induced by neutral, turbulent flow over hills. *Quart. J. Roy. Meteor. Soc.*, **119**, 1233–1267.

—, F. Hewer, and M. Hobson, 1998: *BLASIUS Version 3.03: Documentation of a Model of Flow over Hills*. UK Met Office, 71pp.

Wunsch, C., 1996: *The Ocean Circulation Inverse Problem*. Cambridge University Press, 442pp.

Xu, Z., and A. J. Bowen, 1994: Wave- and wind-driven flow in water of finite depth. *J. Phys. Oceanogr.*, **24**, 1850–1866.

List of Figures

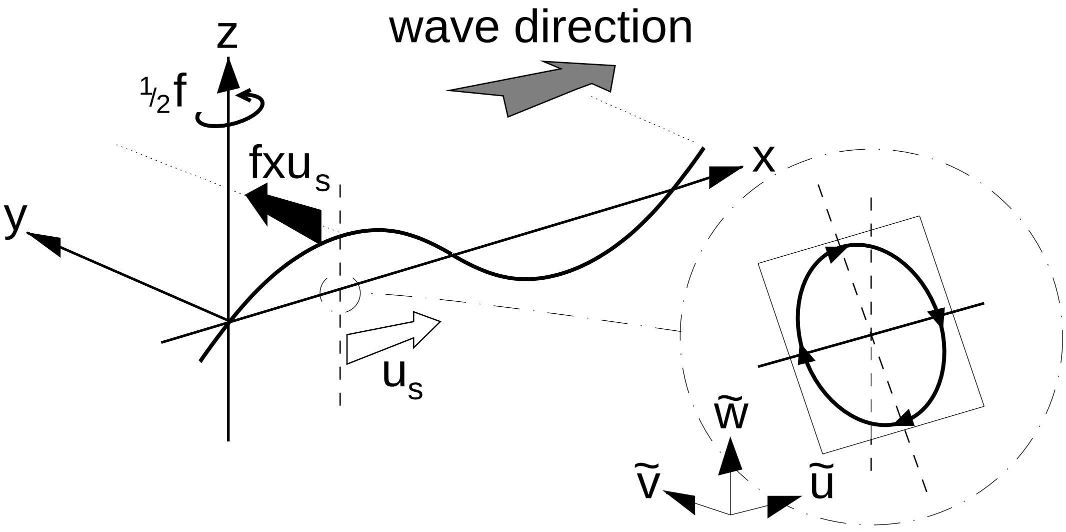

Figure 1: Schematic illustrating the that orbital path for a particle under a wave is tilted, by planetary rotation, in the along wave crest direction. The new $\tilde{v}$ component orbital velocity correlates with the $\tilde{w}$ component to produce a non-zero stress. The divergence of this stress can be written as (Hasselmann 1970) $-\rho \boldsymbol{f} \times \boldsymbol{u_s}$.

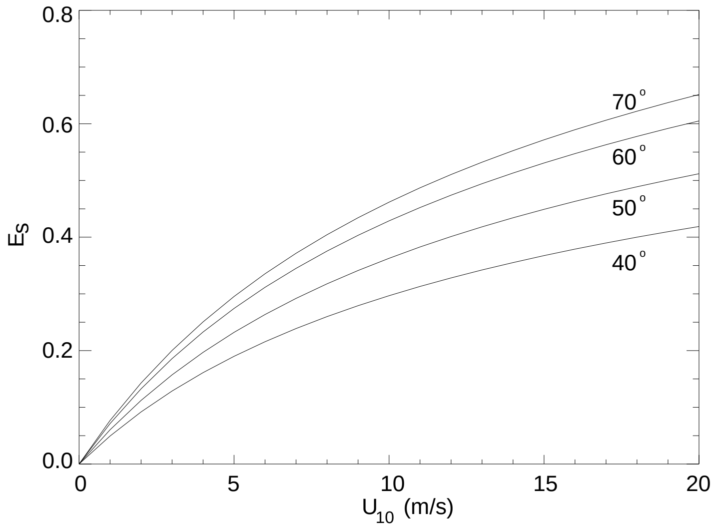

Figure 2: Graph showing how E_s, the ratio of wave-induced to wind-induced transports, varies with U_{10} for 4 different latitudes: $40°, 50°, 60°, 70°$. Even moderate wind speeds of $U_{10} = 12\,\mathrm{m\,s^{-1}}$ suggest wave-induced effects could have a non-negligible impact in the ocean mass transport.

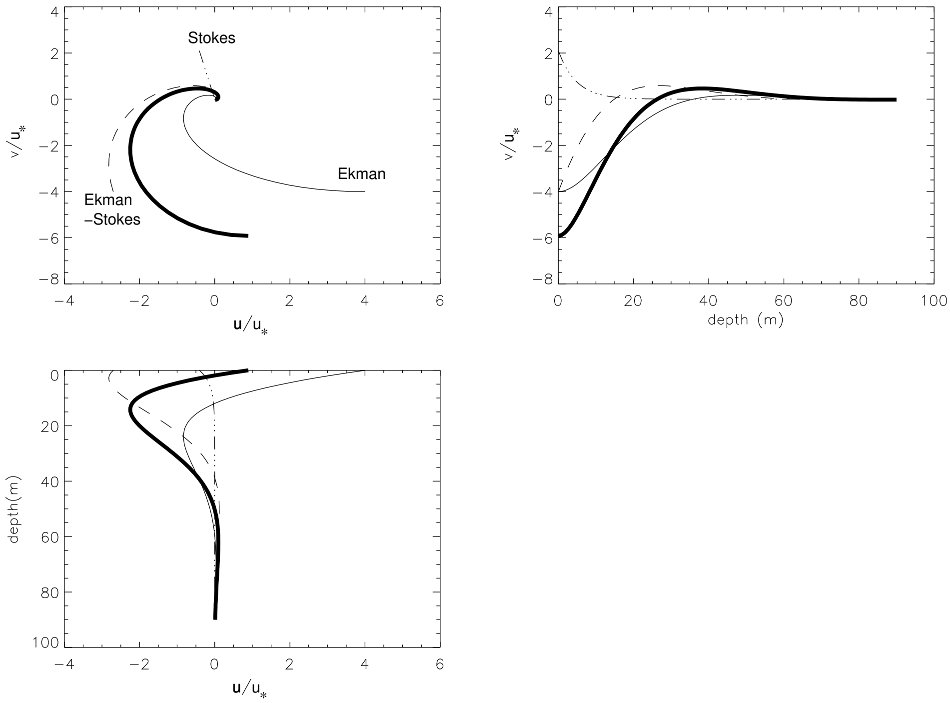

Figure 3: Schematic showing the mean flow velocity components for a solution to the eddy-viscosity closure model with constant eddy viscosity. The parameters are: $\kappa_m = 1.16 \times 10^{-2}\,\mathrm{m}^2\,\mathrm{s}^{-1}$, $u_* = 6.1 \times 10^{-3}\,\mathrm{m\,s}^{-1}$, $f = 1 \times 10^{-4}\,\mathrm{s}^{-1}$, $u_s = 0.068\,\mathrm{m\,s}^{-1}$ and $k = 0.105\,\mathrm{m}^{-1}$ giving depth scales $\delta_e = 15\,\mathrm{m}$ and $\delta_s = 5\,\mathrm{m}$. The thick line is the full solution and the solid thin line is the Ekman component, the dashed line is the Ekman-Stokes component and the dotted-dashed line is the Stokes component. All the velocities are normalised by the friction velocity u_*. The wind stress and wave propagation direction are in the positive x-direction.

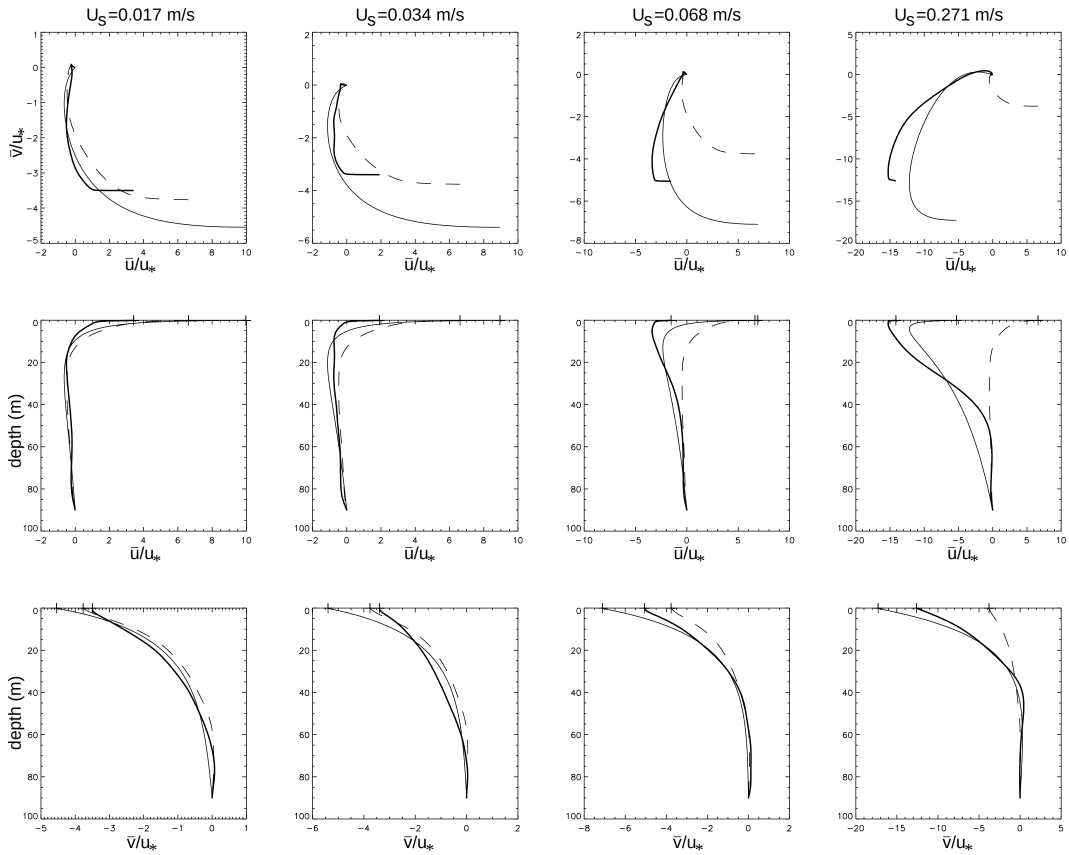

Figure 4: Plots comparing LES solutions with wave forcing (thick solid lines) with LES solutions without wave forcing (thin dashed solid lines) and linear eddy-viscosity closure model solutions (thin solid lines) for a range of U_s and $k = 0.0525\,\mathrm{m}^{-1}$. The upper panels are hodographs of $\bar{v}/u_*$ against $\bar{u}/u_*$ and the middle and lower panels are $\bar{u}/u_*$ and $\bar{v}/u_*$ depth profiles respectively. The eddy-viscosity closure model solution is in remarkably good qualitative agreement with the wave forced LES solution. The wind forcing and wave propagation are both directed along the positive x-axis. With varying U_s, the corresponding wave amplitude a and E_s are: $U_s = 0.017\,\mathrm{m\,s}^{-1}$ ($a = 0.67\,\mathrm{m}$, $E_s = 0.4$), $U_s = 0.034\,\mathrm{m\,s}^{-1}$ ($a = 0.95\,\mathrm{m}$, $E_s = 0.9$), $U_s = 0.068\,\mathrm{m\,s}^{-1}$ ($a = 1.34\,\mathrm{m}$, $E_s = 1.7$) and $U_s = 0.271\,\mathrm{m\,s}^{-1}$ ($a = 2.68\,\mathrm{m}$, $E_s = 6.9$).

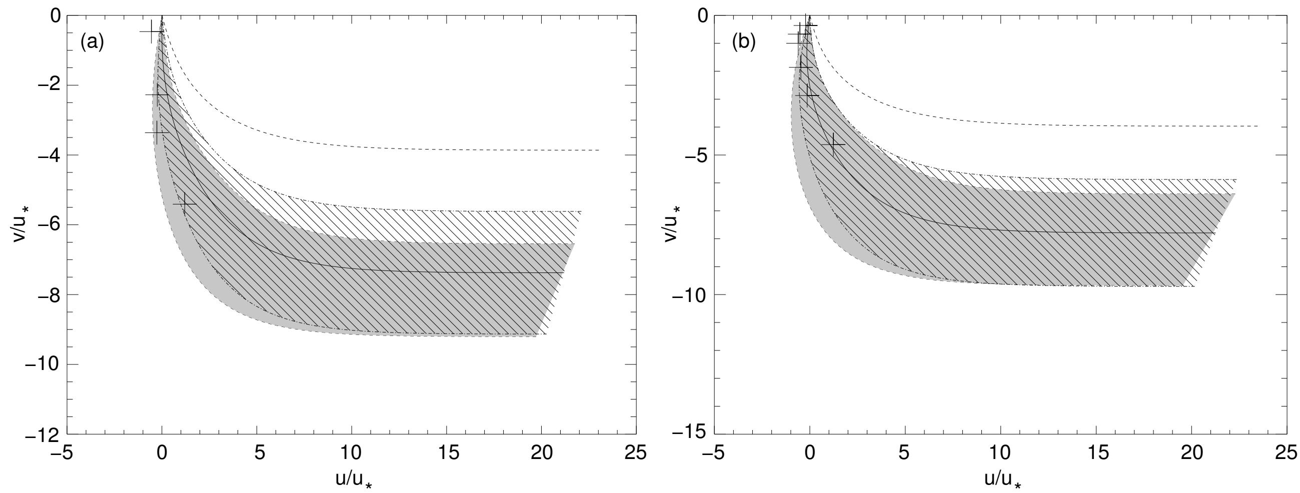

Figure 5: Hodograph comparisons between simple analytic model (assuming a fully developed sea) and observational measurements from (a) LOTUS3 ($u_* = 8.3 \times 10^{-3}\,\mathrm{m\,s^{-1}}$, $z_0 = 1.6 \times 10^{-3}\,\mathrm{m}$) and (b) EBC ($u_* = 9.4 \times 10^{-3}\,\mathrm{m\,s^{-1}}$, $z_0 = 1.4 \times 10^{-3}\,\mathrm{m}$) data sets. Single dash line: model with $u_s = 0$ – no wave effects. Heavy solid line: model with wave effects. Solid shaded envelope: k (from FDS) $\pm 100\%$. Hatched envelope: U_s^2 (that is a^2 from FDS) $\pm 50\%$. Crosses denote observational measurements.